Available online at www.sciencedirect.com
ScienceDirect
Computer Aided Geometric Design 24 (2007) 19–27
COMPUTER AIDED GEOMETRIC DESIGN
www.elsevier.com/locate/cagd

A geometric diagram and hybrid scheme for triangle subdivision

Ángel Plaza [a,*], José P. Suárez [b], Graham F. Carey [c]

[a] *Department of Mathematics, University of Las Palmas de Gran Canaria (ULPGC), Spain*
[b] *Department of Cartography and Graphic Engineering, ULPGC, Spain*
[c] *Institute for Computational Engineering and Sciences (ICES), The University of Texas at Austin, Austin, TX, USA*

Received 14 December 2005; received in revised form 10 July 2006; accepted 5 October 2006

Available online 7 November 2006

Abstract

We introduce a geometrical diagram to study the improvement in shape of triangles generated by iterative application of triangle subdivision. The four Triangles Longest Edge (4TLE) subdivision pattern and a new hybrid 4T Longest-Edge/Self-Similar (hybrid 4TLE-SS) scheme are investigated in this way. The map diagram provides a convenient way to visualize the evolution and migration of element shapes leading to a better understanding of the improvement process and the effect of recursive subdivision schemes. A complex variable mapping analysis supports the diagram and similarity class specifications. Numerical comparisons confirm the superiority of the new hybrid scheme.

Keywords: Geometrical diagram; Mesh improvement; Mesh quality; Triangle subdivision

1. Introduction

Grid generation and, in particular, the construction of 'quality' grids is a major issue in both geometric modeling and engineering analysis (Carey, 1997; Knupp and Steinberg, 1994). Some grid smoothing and optimization strategies are described in (Freitag and Plassman, 2000; Branets and Carey, 2004, 2005; Garimella et al., 2004) and also different mesh quality metrics have been proposed in recent years (Knupp, 2001). In finite element and finite volume methods, acute triangles are favored over obtuse triangles. Many of these methods employ forms of local and global triangle subdivision and seek to maintain well shaped triangles. Here we consider certain triangle subdivision schemes. The self-similar (SS) and 4-triangles longest edge (4TLE) subdivision strategies for triangles are well known (Carey, 1997; Rivara, 1984; Rivara and Iribarren, 1996; Plaza et al., 2004). In the SS scheme the 'parent' triangle is subdivided to a quartet of congruent subtriangles each similar to the parent triangle. Hence, an acute-angled parent triangle will guarantee 4 similar acute subtriangles. Likewise, an obtuse triangle generates 4 similar obtuse subtriangles under SS subdivision. A diagonal swap of the SS internal edge parallel to the longest edge produces the 4TLE pattern (and conversely a swap of the LE bisector will yield the SS pattern). More commonly, the 4TLE partition is constructed by joining the midpoint of the longest edge to the opposite vertex and to the midpoints of the two remaining edges. The

* Corresponding author. Tel.: +34 928 45 88 27; fax: +34 928 45 87 11.
E-mail address: aplaza@dmat.ulpgc.es (Á. Plaza).

0167-8396/$ – see front matter
doi:10.1016/j.cagd.2006.10.002

two subtriangles with edges coincident with the longest edge of the parent are similar to the parent. The remaining two subtriangles form a similar pair that, in general, are not similar to the parent triangle. We refer to such new triangle shapes as 'dissimilar' to those preceding. In the case of a right angled parent triangle all 4 triangles of 4TLE are also SS, and this is the single exception. Note that 4TLE subdivision of an acute triangle yields two acute triangles and two obtuse triangles. Obtuse parent triangles may yield pairs of acute and obtuse triangles or even four obtuse triangles. Repeated recursive subdivision of obtuse triangles under 4TLE will yield meshes that always contain some obtuse subtriangles. However, it has been proven in (Rivara and Iribarren, 1996) that this form of iterative partition of obtuse triangles systematically improves the triangles in the following sense: the sequence of smallest angles monotonically increases, while the sequence of largest angles monotonically decreases in an amount (at least) equal to the smallest angle of each iteration. In addition, bounds on the values of the angles obtained and the exact number of dissimilar triangles have been given in (Plaza et al., 2004).

In the present paper we construct a new geometrical diagram to help interpret and study the migration process for triangle shape under the action of subdivision. The number of dissimilar triangles generated in this way is easily displayed using this diagram. A supporting complex mapping analysis is introduced to define the separators between classes seen in the diagram. Finally, a new hybrid scheme combining the attributes of 4TLE and SS subdivision is developed and shown in numerical experiments to yield superior triangulations.

2. Geometric diagram

The geometric diagram is constructed as follows: (1) For a given triangle or subtriangle the longest edge is scaled to have unit length. This forms the base of the diagram. (2) It follows that the set of all triangles is bounded by this horizontal segment (longest edge) and by two bounding exterior circular arcs of unit radius, as shown in Fig. 1.

In the diagram on the left of Fig. 1 we demarcate shaded regions to classify triangles based on ranges of *largest angle* γ within circular arcs as shown; e.g. the lowermost subregion corresponds to obtuse triangles with large angles near π and the uppermost subregion (exterior to the semicircle of radius $\frac{1}{2}$ centered on the unit base) corresponds to acute-angled triangles. The equilateral triangle corresponds to the apex at $(\frac{1}{2}, \frac{\sqrt{3}}{2})$. As the vertex of a triangle moves from this point along either boundary arc, the maximum angle increases from $\frac{\pi}{3}$ to approach a right angle at the degenerate 'needle triangle' limit near $(0,0)$ or $(1,0)$. Similarly, in the map diagram on the right of Fig. 1 we demarcate by segments of straight lines emanating from $(0,0)$ and $(1,0)$, shaded subregions that bound the *smallest angle* α of a triangle. Color shading makes the respectively subregions easier to identify. The topmost subregion between the exterior circular arcs and the lines for smallest angle $\alpha = \frac{\pi}{4}$ corresponds to triangles with $\frac{\pi}{4} < \alpha < \frac{\pi}{3}$. The v-shaped subregion below this is for $\frac{\pi}{6} < \alpha < \frac{\pi}{4}$ and so on, with the lowest shaded region for $\alpha < \frac{\pi}{12}$. From the shaded regions in these two diagrams, it is clear that slender triangles with large obtuse angles and small acute angles will be located close to the center part of the base and triangles close to equilateral shape will be near the apex of the diagram. It follows that one may be able to use this diagram to investigate the evolution of triangle shapes under subdivision as we show next.

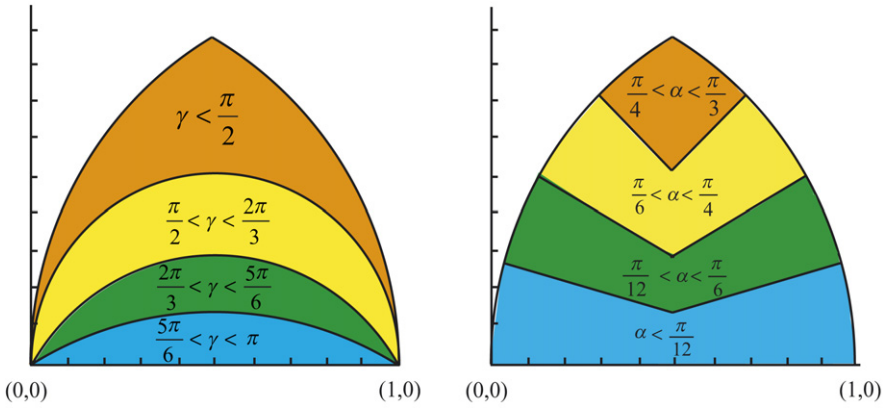

Fig. 1. Diagram for triangles showing different regions corresponding to the largest angle (γ) and the shortest angle (α).

3. Classes of triangles and separators

It is obvious that the right triangle is a separator of the familiar acute and obtuse triangle classes. The locus of points corresponding to this separator is easily identified from elementary geometry as the semicircle with unit diagonal base in our mapping diagram. Points above this semicircle $|z - \frac{1}{2}| = \frac{1}{2}$ correspond to acute triangles and points below correspond to obtuse triangles. We will not show this semicircle in the color class diagrams following, but this property should be kept in mind for other reasons. Here, instead, we focus on the number of dissimilar triangles that are generated by triangle subdivision schemes. As a specific subdivision strategy of general interest, consider the 4TLE strategy. Other schemes such as the hybrid scheme described later also fit naturally in the context of this diagram. In the 4TLE scheme, subdivision leads to subtriangles that are similar to some previous parent triangles in the refinement tree so generated. Other subtriangles may result that are not in such similarity classes yet and we refer to these as new dissimilar triangles. Our goal now is to study the number of dissimilar triangles and classify the triangles in the diagram by this number. To this end, we define the class $\mathcal{C}_n$ as the set of triangles for which the application of the 4TLE partition produces exactly n dissimilar triangles.

Accordingly, let us begin by describing a Monte Carlo computational experiment that can be used to visually distinguish the classes of triangles by the number of dissimilar triangles generated by the 4TLE partition. We proceed as follows: (1) Select a point within the mapping domain comprised by the horizontal segment and by the two bounding exterior circular arcs. This point (x, y) defines the apex of a target triangle. (2) For this selected triangle, 4TLE refinement is successively applied as long as a new dissimilar triangle appears. This means that we recursively apply 4TLE and stop when the shapes of new generated triangles are the same as those already generated in previous refinement steps. (3) The number of such refinements to reach termination defines the number of dissimilar triangles associated with the initial triangle and this numerical value is assigned to the initial point (x, y) chosen. (4) This process is progressively applied to a large sample of triangles (points) uniformly distributed over the domain. (5) Finally, we graph the respective values of dissimilar triangles in a corresponding color map to obtain the result in Fig. 2.

Here, for clarity, the number of dissimilar triangles has been added inside several colored regions to further illustrate the behavior. For instance, the numerical value 2 corresponds to two dissimilar triangles and is associated with the region above the pair of arcs that intersect on the vertical line of symmetry near the point $y = 0.3$. The region below this corresponds to 3 dissimilar triangles, and so on as the base is approached. Viewed another way, obtuse needle-like triangles near the base will require multiple refinements before new dissimilar triangles no longer arise. Later, we will explore this point and plot associated trajectories corresponding to migration of new triangles.

By inspection, of Fig. 2, we deduce that the separator for classes 2 and 3 is given by the segments of two circles of radius $\frac{1}{3}$ centered respectively at $x = \frac{1}{3}$ and $x = \frac{2}{3}$. That is, the curves $|z - \frac{1}{3}| = \frac{1}{3}$ and $|z - \frac{2}{3}| = \frac{1}{3}$. The curves for the subsequent separator between 3 and 4 have slightly more complicated shapes. Moreover, this shape is again evident on two smaller scales at the level of the next separator between 4 and 5. The pattern appears to continue to repeat in

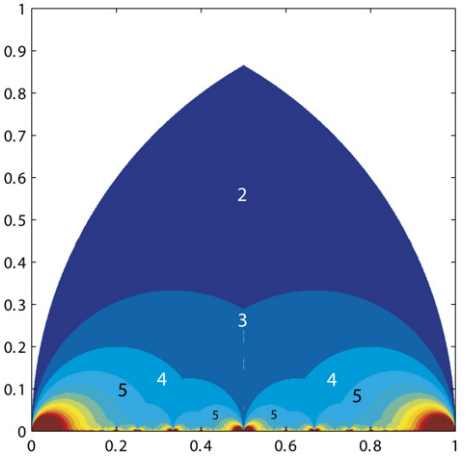

Fig. 2. Subregions for dissimilar triangle classes generated by Monte Carlo simulation.

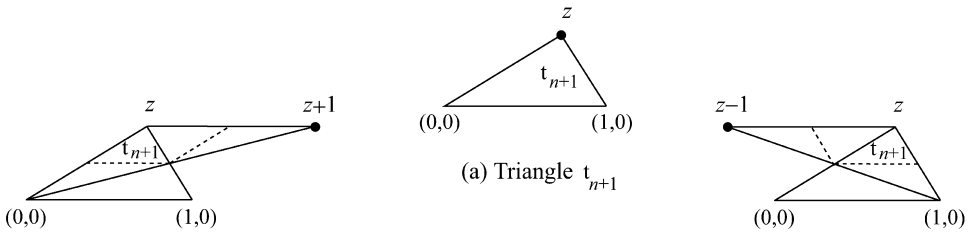

Fig. 3. Two antecedents for the 4TLE partition of triangle t_n.

a fractal like manner as the higher value separators are identified. A more formal mathematical approach, based on mapping in the complex plane, follows and utilizes the concept of antecedent triangle for the 4TLE partition.

4. Complex analysis

Definition 1 *(4TLE Left and Right antecedents).* A given triangle t_{n+1}, has two (different) triangles t_n, denoted here as left and right antecedents, whose 4TLE partition produces triangle t_{n+1}.

As an example, triangle t_{n+1} in the diagram with vertices $(0, 0)$, $(1, 0)$ and z in Fig. 3(a), has left antecedent t_n with vertices z, $(0, 0)$, and $z + 1$ in Fig. 3(b), and right antecedent t_n with vertices z, $(1, 0)$, and $z - 1$ in Fig. 3(c).

Theorem 2. *The relation between the apex of a given triangle z in the right half of the diagram and the apices of its left and right antecedents may be mathematically expressed by the maps $f_L(z) = \frac{1}{\bar{z}+1}$, and $f_R(z) = \frac{1}{2-z}$, complex z.*

Proof. Let t_{n+1} be a triangle determined by its apex vertex z with $Re(z) \geqslant \frac{1}{2}$ and vertices $(0, 0)$ and $(1, 0)$. Left antecedent t_n is given by vertices $(0, 0)$, z and a translate $z + 1$ of z. By geometric transformations shown in Fig. 4, $f_L(z)$ can be derived as follows: apex z is rotated by vector $\vec{w} = \frac{\overline{z+1}}{\|z+1\|}$ so that t_0 is aligned horizontally, as seen in Fig. 4(b–c), and scaled to have normalized longest edge unity, as in Fig. 4(d). A final reflection about the vertical line $x = \frac{1}{2}$ yields the desired antecedent triangle shape with apex in $Re(z) > \frac{1}{2}$, Fig. 4(e). This left antecedent map follows from contraction as $f_L(z) = \frac{1}{\bar{z}+1}$. Complex map $f_R(z) = \frac{1}{2-z}$ is constructed similarly as shown in Fig. 5. □

Remark. Notice that for z having $\frac{1}{2} \leqslant Re(z) \leqslant 1$ then $Re(f_L(z)) \leqslant Re(f_R(z))$ (and hence the 'left'/'right' terminology given to these complex functions).

5. Predecessors of a triangle

To illustrate the use of f_L and f_R, Fig. 6(a) shows a 'trace back' from the equilateral triangle t_0, with apex $(\frac{1}{2}, \frac{\sqrt{3}}{2})$. From equilateral triangle t_0 situated on the intersection of the exterior boundary curves, the only antecedent that generates it after subdivision is triangle t_1. Note that t_1 is an obtuse triangle located exactly where the pair of boundary curves intersect on the vertical line of symmetry at the point $y = \frac{\sqrt{3}}{6}$. Continuing the traceback, this obtuse triangle t_1 is the result of the subdivision of two antecedent triangles as marked, with the right antecedent denoted t_2 and the left one being symmetrically located on the left part of the diagram as expected. Again, each of these t_2 triangles is located at the intersection of two boundary curves. The next pair of antecedents of the right half from left to right are t_3' and t_3 respectively. As before, t_3' and t_3 are located at the intersections of respective pairs of boundary curves that demarcate a change in similarity class and the process continues downward in the diagram with the antecedents approaching the degenerate case of planar obtuse triangles on the horizontal line. Another traceback example is given in Fig. 6(b), starting with apex $(0.67, 0.43)$ (and obviously has a similar path reflected in $x = \frac{1}{2}$).

Theorem 3. *The class separators determined experimentally in Fig.* 2 *may be generated mathematically as a recursive composition of left and right maps $f_L(z)$, and $f_R(z)$.*

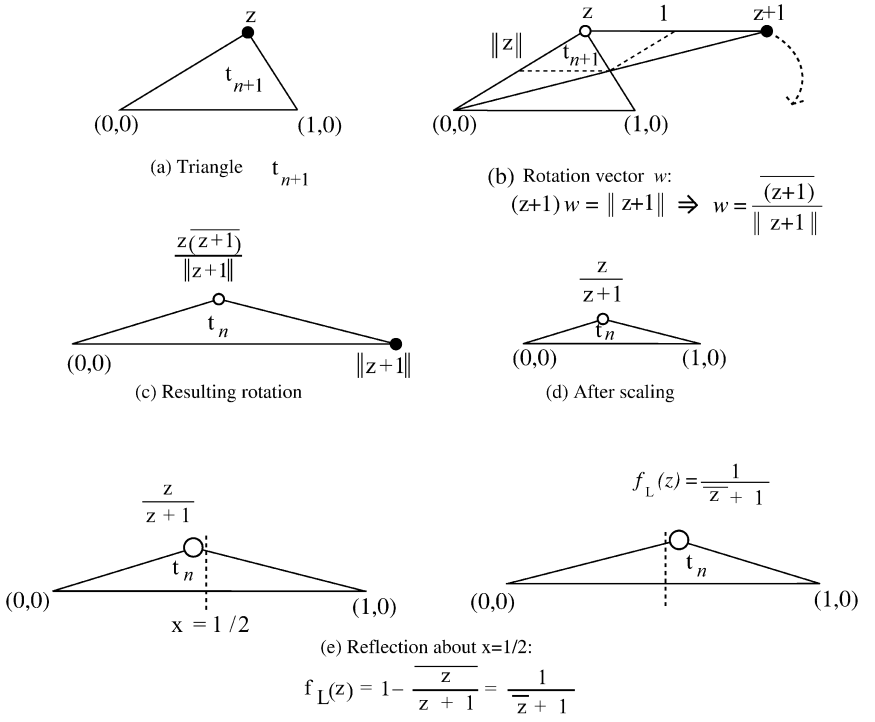

Fig. 4. Geometric transformations to reconstruct the left antecedent t_n of t_{n+1}: $f_L(z)$ for $Re(z) \geqslant \frac{1}{2}$.

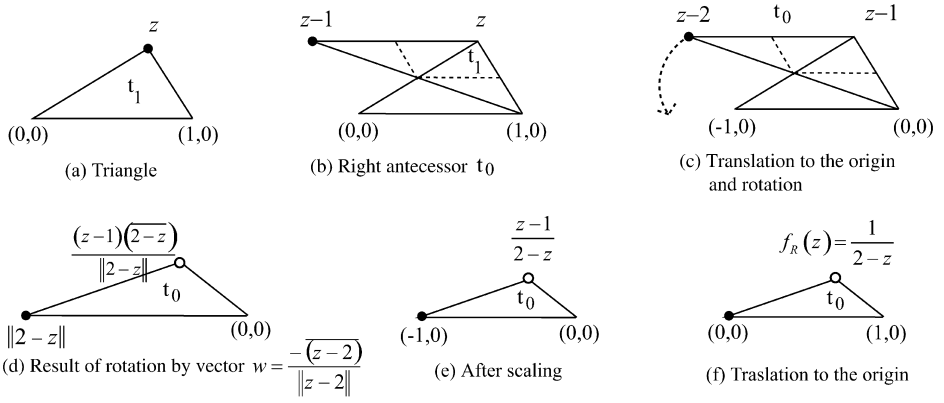

Fig. 5. Geometric transformations to reconstruct the right antecedent t_n of t_{n+1}: $f_R(z)$ for $Re(z) \geqslant \frac{1}{2}$.

Proof. Transformations f_L and f_R can be used to determine the equations of class separator curves in the diagram. Beginning with the boundary curves, consider the circular arc defined by $|z| = 1$ for $x > \frac{1}{2}$ on the right part of the diagram. The successive application of transformation f_R gives the following sequence of arcs:

$$\left|z - \frac{2}{3}\right| = \frac{1}{3}; \quad \left|z - \frac{4}{5}\right| = \frac{1}{5}; \quad \ldots; \quad \left|z - \frac{2n}{2n+1}\right| = \frac{1}{2n+1}$$

all passing through the point $(1, 0)$ and with decreasing radius. Note also that by applying transformation f_L to the previous sequence of arcs, the reflected arcs are obtained:

$$\left|z - \frac{5}{8}\right| = \frac{1}{8}; \quad \left|z - \frac{9}{16}\right| = \frac{1}{16}; \quad \ldots; \quad \left|z - \frac{4n+1}{8n}\right| = \frac{1}{8n}$$

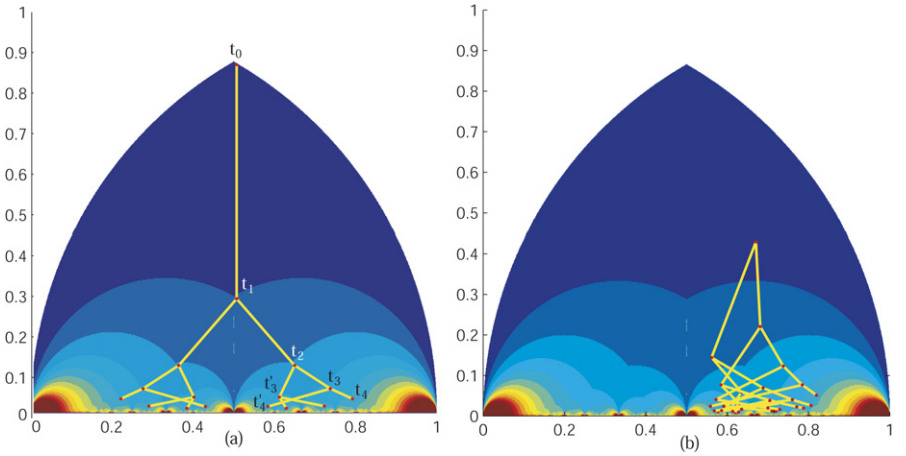

Fig. 6. Traceback curves showing antecedents in successive regions: (a) traceback from equilateral triangle apex with antecedents on border curves and (b) traceback from acute triangles interior to region.

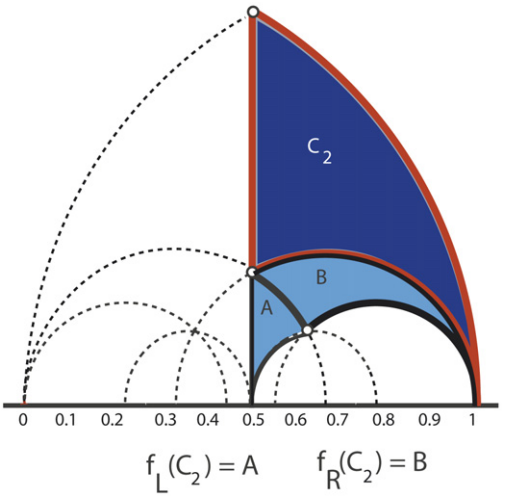

Fig. 7. Boundary curves for $\mathcal{C}_2$ and $\mathcal{C}_3 = A \cup B$.

Since we are particularly interested in the border curves for dissimilar classes, let C_n and $\partial\mathcal{C}_n$ denote the set and its boundary of apices of triangles generating exactly n dissimilar triangles. Since $\mathcal{C}_{n+1} = f_L(\mathcal{C}_n) \cup f_R(\mathcal{C}_n)$, the boundary $\partial\mathcal{C}_{n+1}$ is obtained by the images through f_L and f_R of $\partial\mathcal{C}_n$: $\partial\mathcal{C}_{n+1} = \partial(f_L(\mathcal{C}_n) \cup f_R(\mathcal{C}_n)) \subset f_L(\partial\mathcal{C}_n) \cup f_R(\partial\mathcal{C}_n)$. This result is indicated in our diagram in Fig. 7 for $n = 2$ with the region corresponding to 2 dissimilar triangles, equivalence class $\mathcal{C}_2$, shown in dark shade. Application of mapping functions f_R and f_L yields a new region shown in lighter shade. This region corresponds to equivalence class $\mathcal{C}_3$ and is composed of two parts: $f_L(\mathcal{C}_2) = A$ and $f_R(\mathcal{C}_2) = B$ as shown. A progressive set of subregions (and interfaces) can be obtained similarly, with:

$$\mathcal{C}_2 = \left\{ z/\frac{1}{2} \leqslant Re(z) \leqslant 1;\ |z| \leqslant 1;\ \left| z - \frac{2}{3} \right| \geqslant \frac{1}{2} \right\}$$

$$\mathcal{C}_3 = f_L(\mathcal{C}_2) \cup f_R(\mathcal{C}_2)$$

$$\vdots$$

$$\mathcal{C}_n = f_L(\mathcal{C}_{n-1}) \cup f_R(\mathcal{C}_{n-1})$$

That is, the set $\mathcal{C}_n$ (and correspondingly $\partial\mathcal{C}_n$) is obtained by $n-1$ repetitive applications of f_L and f_R to $\mathcal{C}_2$. □

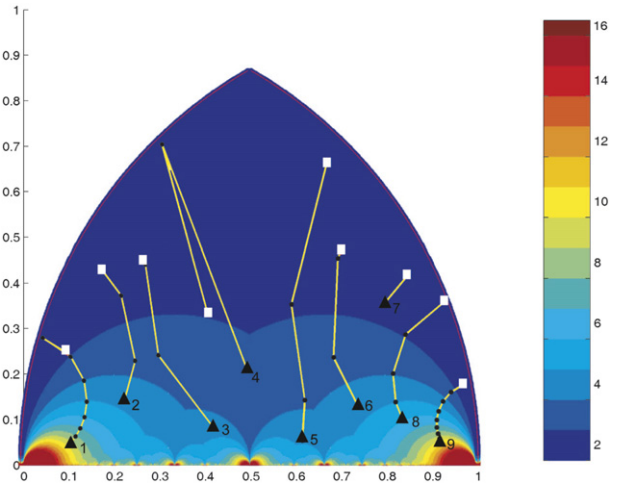

Fig. 8. Trajectories for a sample of triangles.

6. Migration trajectories

In the diagram, each triangle is identified by its apex. By joining the successive apex vertices of consecutive triangles, we get a migration trajectory that visually depicts the improvement of the triangles. The migration trajectories for a sample of 9 triangles are shown in Fig. 8. Here, each trajectory begins from an initial triangle labelled with a number and a solid triangle symbol. Each new dissimilar triangle type is marked on the trajectory by a small dark circle, and the last dissimilar triangle after several subdivisions is marked by an open square.

Hence we see that the scheme tends to generate improved new elements as indicated by the upward migration paths. We can express the behavior along the trajectories more formally in terms of a directed sequence chart as follows:

Consider an initial obtuse triangle. Iterative 4TLE subdivision from this initial triangle produces a finite sequence of 'better' triangles satisfying the properties illustrated in the following diagram: until triangle t_N becomes non-obtuse (Rivara and Iribarren, 1996; Plaza et al., 2004),

$$\begin{array}{ccccccc} t_0 & \to & t_1 & \to & t_2 & \to \cdots \to & t_N \\ \text{(obtuse)} & & \text{(obtuse)} & & \text{(obtuse)} & & \text{(non-obtuse)} \\ \alpha_0 & & \alpha_1 > \alpha_0 & & \alpha_2 > \alpha_1 & & \alpha_N > \alpha_{N-1} \\ \beta_0 & & \beta_1 > \beta_0 & & \beta_2 > \beta_1 & & \beta_N > \beta_{N-1} \\ \gamma_0 & & \gamma_1 \leqslant \gamma_0 - \alpha_1 & & \gamma_2 \leqslant \gamma_1 - \alpha_2 & & \gamma_N \leqslant \gamma_{N-1} - \alpha_N \end{array}$$

where α_i, β_i, and γ_i are the three angles of triangle t_i in increasing order. The arrow emanating from triangle t_i to triangle t_{i+1} means that the (first) 4TLE partition of triangle t_i produces the new dissimilar triangle t_{i+1}. Triangle t_{i+1} is called the successor of t_i, while t_i will be called the antecedent of t_{i+1}. This improvement in the shape of the generated triangles from an initial obtuse triangle t_0 is also displayed by the trajectories in Fig. 8. Moreover, the process described in the preceding sequence inevitably results in one of the situations illustrated below (Rivara and Iribarren, 1996):

$$\begin{array}{lccccc} (1) & t_{N-1} & \rightleftharpoons & t_N & & \gamma_{N-1} + \gamma_N = \pi \\ & \text{obtuse} & & \text{non-obtuse} & & \\ (2) & t_{N-1} & \to & t_N \circlearrowleft & & \gamma_N = \pi/2 \\ & \text{obtuse} & & \text{right-angled} & & \\ (3) & t_{N-1} & \to & t_N & \rightleftharpoons \; t_{N+1} & \gamma_N + \gamma_{N+1} = \pi \\ & \text{obtuse} & & \text{non-obtuse} & \text{obtuse} & \end{array}$$

This behavior is confirmed visually by the sample trajectories in our diagram. For instance, notice in Fig. 8, situation (1) $t_{N-1} \rightleftharpoons t_N$ arises for trajectories 2, 5, and 8; situation (2) $t_{N-1} \to t_N \circlearrowleft$ occurs at the end of the trajectories 3 and 6. Finally, note that 'reversals' at the end of the trajectories, as in situation (3) are also possible with this scheme, as seen in Fig. 8 (see trajectories 1 and 4) but do not occur in the hybrid scheme discussed next.

Table 1
Percent of acute triangles for an initial obtuse triangle and 9 refinement steps

Refin.	Triangle t_3		Triangle t_4		Triangle t_5	
level N	4Thybrid	4TLE	4Thybrid	4TLE	4Thybrid	4TLE
1	0.0	0.0	50.0	50.0	0.0	0.0
2	25.0	25.0	75.0	50.0	0.0	0.0
3	50.0	37.5	87.5	50.0	12.5	12.5
4	68.7	43.7	93.7	50.0	31.1	25.0
5	81.2	46.8	96.9	50.0	50.0	34.4
6	89.0	48.4	98.4	50.0	65.6	40.6
7	93.7	49.3	99.2	50.0	77.3	44.5
8	96.4	49.6	99.6	50.0	85.5	46.9
9	98.0	49.8	99.8	50.0	91.0	48.2

7. Hybrid 4TLE/SS subdivision

SS subdivision generates no new dissimilar elements, so the mapping under SS in the diagram at each recursion is an identity. Since acute triangles are preserved under SS, one may devise a hybrid strategy (hybrid 4TLE-SS) that invokes 4TLE on obtuse triangles and SS on acute triangles. Obviously, this strategy generates a different refinement than either SS or 4TLE. Under this hybrid scheme, SS refinement of acute triangles reproduces the same points in the diagram. These points all lie in the uppermost shaded region on the left of Fig. 1. 4TLE refinement of obtuse triangles may generate acute triangles, thereby defining a migration to the same region on the left of Fig. 1. This implies that, under the hybrid scheme, there will be no reversals similar to those seen in Fig. 8.

Since 4TLE refinement of an acute triangle will produce a pair of obtuse subtriangles, we anticipate the hybrid scheme will be superior in the sense that it will lead to meshes with more acute triangles. We explore this numerically in the next test by selecting a representative sample of obtuse initial triangles from those used to generate the 9 trajectories in Fig. 8. Each of the triangles in our sample is recursively refined through 9 levels using 4TLE and hybrid subdivision, respectively. The percentage of acute triangles at each level can then be compared, as can the growth in number of acute triangles with refinement level. These percentages for the 3 initial triangles marked as 3, 4, 5 at the starting points of the corresponding trajectories in Fig. 9 are given in Table 1. Level $N = 1$ corresponds to the first refinement to 4 subtriangles, level 2 is the next refinement level with 16 subtriangles, and so on with 4^N subelements at level N. Note that there will always be *at least* 2^N obtuse triangles on the base when 4TLE is applied (even in the hybrid scheme) so *an upper bound* on the percentage of acute triangles follows trivially as $[1 - \frac{2^N}{4^N}] \cdot 100\%$. This result is closely approached in the accompanying numerical tests with the hybrid scheme.

We see from the table that the percentage of acute triangles for the standard 4TLE scheme approaches 50% as N increases, whereas the hybrid scheme rapidly approaches values close to 100% by 7 levels. For obtuse isosceles triangle t_3 at level 4, inspection confirms that obtuse triangles persist only along the bottom edge of the original macroparent triangle when the hybrid scheme is applied. On the other hand, obtuse triangles are generated and persist in the interior under the uniform 4TLE subdivision scheme. (Remark: It is relatively straightforward to augment the subdivision strategy and remove the obtuse angles in the hybrid case for this isosceles triangle t_3, by completion with longest edge bisection (2TLE) for the base elements on this macroparent edge. In general such a simple solution is not feasible. Other schemes that involve local node insertion edge swapping, or local mesh smoothing may be applied (e.g. Edelsbrunner and Shah, 1992; Freitag and Plassman, 2000; Canann et al., 1993; Ohtake et al., 2001). However, these aspects of mesh improvement are not the objective of the present study.

8. Conclusions

A new diagram is introduced to facilitate studies of triangle shape evolution under subdivision strategies, and a Monte Carlo experiment maps out subregions in the diagram that delineate different similarity classes. This motivates a mathematical proof using complex valued maps to construct the border curves for these regions in the diagram. The maps also yield trajectory paths that are used to describe the migration of element shape under recursive refinement. These trajectories are then used to visually interpret the behavior described by terminating sequences that were intro-

duced in prior work. A new hybrid subdivision scheme is proposed, and the diagram is applied to infer the comparative behavior of 4TLE and hybrid 4TLE-SS recursive subdivision. Tabulated comparative results for the percentages of acute triangles are obtained from a related numerical experiment. These confirm that the hybrid 4TLE-SS strategy dramatically accelerates the approach towards an acute triangulation.

Acknowledgements

This work has been supported in part by Project UNI-2003/35 from University of Las Palmas de Gran Canaria, by CYCIT Project number MTM2005-08441-C02-02 from Ministerio de Educacion y Ciencia of Spain, and by Sandia and Los Alamos DOE Laboratories. The second author wants to thank Gobierno de Canarias, ICES and the CFDLab for their financial support during his stay at the University of Texas at Austin.

References

Branets, L., Carey, G.F., 2004. Smoothing and adaptive redistribution for grids with irregular valence and hanging nodes. In: Proceedings of the 13th International Meshing Roundtable.

Branets, L., Carey, G.F., 2005. A local cell quality metric and variational grid smoothing algorithm. Engrg. Comp. 21 (1), 19–28.

Canann, S., Stephenson, M., Blacker, T., 1993. Optismoothing: an optimization-driven approach to mesh smoothing. Finite Elements in Analysis and Design 13 (2–3), 185–190.

Carey, G.F., 1997. Computational Grids: Generation, Refinement and Solution Strategies. Taylor and Francis.

Edelsbrunner, H., Shah, N., 1992. Incremental topological flipping works for regular triangulations. In: Proceedings of the 8th ACM Symposium on Computational Geometry, pp. 43–52.

Freitag, L.A., Plassman, P., 2000. Local optimization-based simplicial mesh untangling and improvement. Int. J. Num. Meth. Engrg. 49 (1), 109–125.

Garimella, R.V., Shashkov, M.J., Knupp, P.M., 2004. Triangular and quadrilateral surface mesh quality optimization using local parametrization. Comp. Meth. Appl. Mech. Engrg. 193 (9–11), 913–928.

Knupp, P.M., Steinberg, S., 1994. The Fundamentals of Grid Generation. CRC Press, Boca Raton, FL.

Knupp, P.M., 2001. Algebraic mesh quality metrics. SIAM J. Sci. Comput. 23, 193–218.

Ohtake, Y., Belyaev, A., Bogaevski, I., 2001. Mesh regularization and adaptive smoothing. Computer-Aided Design 33 (11), 789–800.

Plaza, A., Suárez, J.P., Padrón, M.A., Falcón, S., Amieiro, D., 2004. Mesh quality improvement and other properties in the four-triangles longest-edge partition. Computer Aided Geometric Design 21 (4), 353–369.

Rivara, M.-C., 1984. Algorithms for refining triangular grids suitable for adaptive and multigrid techniques. Inter. J. Num. Meth. Engrg. 20, 745–756.

Rivara, M.-C., Iribarren, G., 1996. The 4-triangles longest-side partition of triangles and linear refinement algorithms. Math. Comp. 65 (216), 1485–1502.